NASA TECHNICAL NOTE

NASA TN D-5720

NASA TN D-5720

GAS JET IMPINGEMENT ON LIQUID SURFACES DURING WEIGHTLESSNESS

by Thomas L. Labus

Lewis Research Center

Cleveland, Ohio

NATIONAL AERONAUTICS AND SPACE ADMINISTRATION • WASHINGTON, D. C. • MARCH 1970

1. Report No. NASA TN D-5720	2. Government Accession No.	3. Recipient's Catalog No.
4. Title and Subtitle GAS JET IMPINGEMENT ON LIQUID SURFACES DURING WEIGHTLESSNESS		5. Report Date March 1970 6. Performing Organization Code
7. Author(s) Thomas L. Labus		8. Performing Organization Report No. E-5438
9. Performing Organization Name and Address Lewis Research Center National Aeronautics and Space Administration Cleveland, Ohio 44135		10. Work Unit No. 124-09 11. Contract or Grant No. 13. Type of Report and Period Covered Technical Note
12. Sponsoring Agency Name and Address National Aeronautics and Space Administration Washington, D.C. 20546		14. Sponsoring Agency Code

15. Supplementary Notes

16. Abstract

As part of the continuing research into the behavior of liquids in weightlessness, an experimental drop-tower investigation was conducted to determine the characteristics of a laminar gas jet impinging normally on a liquid surface during weightlessness. Surface penetration depths from a gas that exited from a circular nozzle with an initially parabolic velocity profile were correlated in terms of known system parameters. Contact angles on the test container surfaces were restricted to 90^{o} so that the liquid-gas interface remained flat during impingement. Also included are qualitative observations concerning the resulting cavity shape, bubble pinch-off, and, for the case of large gas jet momentums, cavity growth.

17. Key Words (Suggested by Author(s))		18. Distribution Statement
Laminar	Impingement	Unclassified - unlimited
Gas	Liquids	
Jets	Weightlessness	

19. Security Classif. (of this report)	20. Security Classif. (of this page)	21. No. of Pages	22. Price*
Unclassified	Unclassified	25	$3.00

*For sale by the Clearinghouse for Federal Scientific and Technical Information Springfield, Virginia 22151

GAS JET IMPINGEMENT ON LIQUID SURFACES DURING WEIGHTLESSNESS

by Thomas L. Labus

Lewis Research Center

SUMMARY

As part of the continuing research into the behavior of liquids in weightlessness, an experimental drop-tower investigation was conducted to determine the characteristics of a laminar gas jet impinging normally on a liquid surface during weightlessness. Surface penetration depths from a gas that exited from a circular nozzle with an initially parabolic velocity profile were correlated in terms of known system parameters. Contact angles on the test container surfaces were restricted to 90^{o} so that the liquid-gas interface remained flat during impingement. Also included are qualitative observations concerning the resulting cavity shape, bubble pinch-off, and, for the case of large gas jet momentums, cavity growth.

INTRODUCTION

The NASA Lewis Research Center has been conducting basic and applied research to study the static and dynamic behavior of liquids under reduced gravitational conditions. As part of this research program, the problems associated with the dynamic effects of a gas jet impinging on a liquid surface are of interest. In general, pressurization systems, whether used in normal gravity, reduced gravity, or weightlessness, must be designed to function properly in their environment. Cases in which pressurization techniques result in a gas or vapor jet impinging on a liquid surface require a knowledge of the dynamic effects of the jet and the resulting interaction with the liquid surface in order to predict gas penetration, spraying, free bubble motion in the liquid, and gas blowthrough. Such pressurization systems are encountered for a wide variety of applications, ranging from the effect of a pressurant gas on a liquid draining from its container to the effect of a rocket exhaust gas on the surface of a body of water during lift-off.

A number of studies have been conducted in which the dynamics of gaseous jets impinging on liquid surfaces were examined under normal gravity conditions. In reference 1, both an analytical and an experimental investigation were conducted under normal gravity conditions. The authors analytically considered circular and plane (two-

dimensional) jets with both free-streamline and turbulent flows. The results of their experiments, which employed turbulent jets, showed good agreement with the proposed normal gravity theory. Turbulent jets in a normal gravity environment were studied experimentally in reference 2, which gives an excellent discussion of the types of instability that may occur under normal gravity conditions, including bubble entrainment and high amplitude sloshing. Turbulent gas jets impinging normally on liquid surfaces under normal gravity conditions (ref. 3) were the subject of a study oriented to predicting penetration depths due to the exhaust of space vehicles launched from platforms built over a water surface. Analytical investigations of two-dimensional potential jets have also been conducted (ref. 4). With the exception of an analysis conducted in reference 1, no analytical or experimental information is presently available concerning gas impingement in weightlessness, where the effects of surface tension forces must be included. A logical extension of the experimental normal gravity studies would, therefore, be to examine the gas impingement phenomena during zero gravity (weightless) conditions. This investigation is restricted to the study of laminar gas jets with initially parabolic profiles such that the jet momentum and centerline velocity are known.

The purpose of this report is to present the results of an experimental investigation conducted at the NASA Lewis Research Center on gas impingement phenomena under weightless conditions using laminar parabolic jets. Contact angles were restricted to 90° so that the liquid-gas interface was flat during weightlessness. The distance between the liquid surface and the nozzle tip was restricted to less than three nozzle diameters to minimize jet spreading. The data obtained on penetration depths for laminar parabolic jets are presented and correlated in terms of known system parameters. The analytical considerations, extending the initial work conducted by Banks et al. (ref. 1), are, in general, verified by the experimental data. Also presented are qualitative observations concerning the resulting cavity shape, bubble pinch-off, and cavity growth at large jet momentums.

SYMBOLS

a_o cross-sectional area of nozzle, cm^2

d_o nozzle diameter, cm

H distance between nozzle tip and liquid surface, cm

h_p penetration depth into liquid measured along axis of symmetry, cm

L nozzle length, cm

M jet momentum flux, dynes; N

n_o	coordinate along axis of symmetry, cm
p	pressure, dynes/cm^2; N/cm^2
R	nozzle radius, cm
Re	Reynolds number, Re = $\overline{V}_J d_o/\nu_g$
R_o	radius of curvature at stagnation point, cm
r	coordinate measured perpendicular to axis of symmetry, cm
t	time, sec
V_J	jet velocity, cm/sec
$V_{J,max}$	maximum jet velocity, cm/sec
$\overline{V}_J$	average jet velocity, cm/sec
β	theoretical constant
μ	viscosity, cP; (N)(sec)/m^2
ν	kinematic viscosity, μ/ρ, cm^2/sec
ρ	density, g/cm^3
σ	surface tension, dynes/cm; N/cm

Subscripts:

g	gas
l	liquid
par	parabolic profile

ANALYSIS

Gas Impingement Model

The assumed mathematical model is an axisymmetric gas cavity located directly below a circular nozzle. A schematic drawing showing the parameters of the model is presented in figure 1. In the model, an incompressible, inviscid gaseous jet with a known velocity profile interacts with a liquid surface of infinite extent; the gaseous jet in this model, therefore, is a free-streamline jet. The jet penetrates the liquid surface at right angles and forms a smooth gas cavity under steady-state conditions. A two-dimensional coordinate system is chosen with an origin located at the point 0 (as shown in fig. 1), where r and n_o are defined as the coordinates of the axisymmetric liquid surface. The

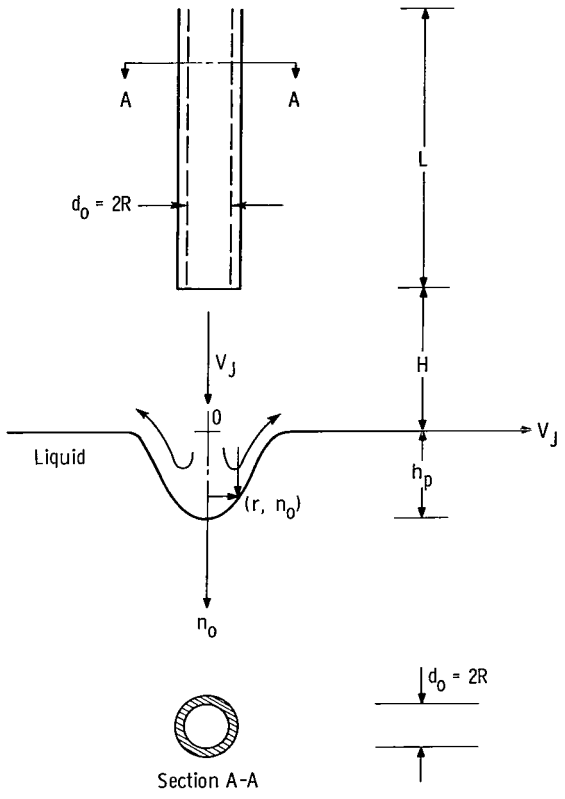

Figure 1. - Defining variables in gas impingement study.

liquid has a surface tension σ_l and a density ρ_l and is initially located at a distance H from the nozzle and at right angles to it. Because the liquid surface is assumed to be of infinite extent, the gas penetration that results in a cavity will not appreciably affect the distance H. The gas has a density ρ_g and is traveling with some velocity V_J, which depends on its initial velocity profile and distance from the centerline. The lowest point on the liquid-gas interface is the position at which the jet velocity is zero and is defined as the stagnation point. While the distance H will not affect a solution using an inviscid model, in experimental applications it should be kept as small as possible to minimize jet spreading. The penetration depth into the liquid surface measured along the axis of symmetry and locating the stagnation point is defined as h_p. By means of this model, equations are developed to predict the penetration depth into the liquid surface as a function of both liquid and gas parameters.

For a circular nozzle of diameter d_o, Boussinesq's formula (ref. 5) shows that the exiting velocity profile will be a function of the nozzle length and the Reynolds number. Initially, the velocity profile entering the nozzle will be irregularly shaped, but as the length of the nozzle increases, the profile approaches a completely developed parabolic

profile commonly known as Hagen-Pouiselle flow. Parabolic profiles prevail if the following condition is met:

$$\frac{L}{d_o} \geq 0.0145\ \mathrm{Re} \tag{1}$$

where

$$\mathrm{Re} = \frac{\overline{V}_J d_o}{\nu_g}$$

From reference 6, for the case of a fully established parabolic flow, the maximum jet velocity along the centerline $V_{J,max}$ is twice the average jet velocity, as determined by mass conservation laws. The momentum flux for a gaseous jet possessing a completely parabolic profile is

$$M_{par} = \frac{4}{3} \rho_g a_o \overline{V}_J^2 \tag{2}$$

where a_o is the cross-sectional area of the circular nozzle.

Governing Equations

Both references 1 and 2 indicate how the surface tension effects of a gas jet penetrating a liquid surface can be treated. Reference 1 made some calculations for turbulent spreading jets in order to correct some of their normal gravity data. In a weightless or zero-gravity environment, surface tension is the only force that enables the formation of a stable gas cavity, shown in figure 1, and, therefore, the following analysis is applicable. Bernoulli's equation is applied along a streamline between the stagnation point and some point along the jet centerline in the region of the liquid-gas interface. The following equation is obtained in weightlessness, as demonstrated by both references 1 and 2:

$$\frac{1}{2} \rho_g V_J^2 = \frac{2\sigma}{R_o} \tag{3}$$

where

ρ_g density of gas, g/cm^3

V_J jet velocity along centerline in region of liquid-gas interface, cm/sec

σ surface tension, dynes/cm; N/cm

R_o radius of curvature at stagnation point, cm

However, in order to evaluate equation (3), the radius of curvature R_o must be determined. The term R_o must be found from the shape of the gas cavity. A method similar to that employed by Banks et al. for square profiles and turbulent jets appears to be one approach to obtaining the cavity shape.

Cavity shape. - A gas impinging on a liquid surface results in a pressure distribution along that surface. When a gaseous jet with an initially parabolic velocity profile is considered, the integrated pressure distribution on the surface is balanced by the momentum flux

$$\frac{4}{3}\rho_g a_o \overline{V}_J^2 = 2\pi \int_0^\infty pr\, dr \tag{4}$$

An error curve approximation for the pressure distribution on the liquid surface was obtained in reference 1 by empirically correlating experimental data measured on a flat plate from reference 7. However, the form of the pressure distribution of reference 1 appears applicable only for laminar circular jets possessing initially flat velocity profiles, whereas the present analysis is concerned with parabolic profiles. Since no experimental or analytical information is available that might yield the pressure distribution on a flat plate for the case of a parabolic profile, an approach similar to the error curve approximation was taken with the following modification: The pressure was nondimensionalized with respect to the term $2\rho_g \overline{V}_J^2$, the maximum static pressure for the case of a completely developed parabolic profile, and the following equation was obtained:

$$\frac{p}{2\rho_g \overline{V}_J^2} = e^{-\beta(r/d_o)^2} \tag{5}$$

Substitution of equation (5) into equation (4) yields a value of 6 for the constant β. Therefore, the following equation was obtained for the pressure distribution for laminar circular jets impinging on liquid surfaces with initially parabolic velocity profiles when H/d_o is small; that is, the jet has not yet begun to spread appreciably:

$$\frac{p}{2\rho_g \overline{V}_J^2} = e^{-6(r/d_o)^2} \tag{6}$$

A further assumption in the analysis is that, when the cavity depression is sufficiently small, the change in shape of the liquid surface does not appreciably alter the velocity and pressure distribution of the gas flow. Assuming that the cavity response or depression will follow the calculated pressure distribution, one obtains the following expression for the surface shape:

$$\frac{n_o}{h_p} = e^{-6(r/d_o)^2} \tag{7}$$

With reference to equation (3), the radius of curvature at the stagnation point can now be evaluated from equation (7). The radius of curvature is defined as

$$R_o = \frac{\left[1 + (n_o')^2\right]^{3/2}}{n_o''} \tag{8}$$

where the primes indicate differentiation with respect to r. Substitution of equation (7) into equation (8) yields

$$|R_o| = \frac{d_o^2}{12h_p} \qquad \text{at} \quad r = 0$$

Depth of penetration relations. - Substitution of R_o into Bernoulli's equation for weightlessness (eq. (3)), therefore, yields

$$\frac{1}{2}\rho_g V_J^2 = 24\frac{\sigma h_p}{d_o^2} \tag{10}$$

After substitution of $\overline{V}_J = \frac{1}{2} V_J$, equation (10) can be rewritten as

$$\rho_g \left(d_o \overline{V}_J\right)^2 = 12(\sigma h_p) \tag{11}$$

In terms of the momentum flux, equation (11) becomes

$$M_{par} = 4\pi(\sigma h_p) \tag{12}$$

Both equations (11) and (12) predict the penetration depth in weightlessness for laminar gas jets possessing initially parabolic velocity profiles.

APPARATUS AND PROCEDURE

A detailed description of the 2.2-Second Zero-Gravity Facility and the experimental apparatus and procedure used is given in the appendix. Briefly, the experimental investigation utilized a flat-bottomed, 19-centimeter-diameter, cylindrical container filled with the test liquid, distilled water. A circular brass nozzle with an inside diameter of either 0.127 or 0.254 centimeter was located above the liquid surface and at right angles to it. Nitrogen was used as the test gas that passed through the brass nozzle and subsequently impinged on the liquid surface. The physical properties of both the gas and the liquid were calculated at 20° C. The density of the gas was calculated at atmospheric pressure since the gas excited into atmospheric air. The contact angle that the liquid surface makes with the test container surface was maintained at 90° (as described in the appendix) so that the liquid-gas interface remained flat during weightlessness. A more complete description of both nozzles and the test container is given in the appendix.

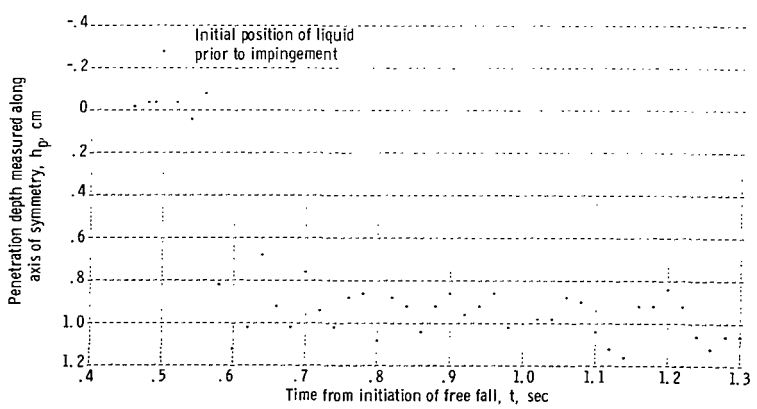

Figure 2. - Sample data plot of gas impingement.

DATA REDUCTION

The motion of the liquid-gas interface during impingement was recorded for each test

on motion picture film. From the film, the penetration depths measured along the jet centerline were obtained as functions of test time. A sample plot is shown in figure 2. With the use of a computer, the average penetration depth was then calculated for each data run.

RESULTS AND DISCUSSION

Description of Gas Impingement Phenomena

Prior to making a comparison between the experiments and the theoretical considerations described in the previous section, it is worthwhile to examine the behavior of the gas impingement phenomena in weightlessness and to compare it with normal gravity behavior. Such a comparison is shown in figure 3. The relative penetration depth in weightlessness is considerably greater than in normal gravity because of the absence of the gravitational restraining forces. Other important features commonly observed in normal gravity occur when the gas momentum is sufficiently large, and a condition commonly called "spraying" or "sputtering" is observed. This condition results in the dispersion of liquid droplets from the surface into surrounding gas and is accompanied by both lateral and vertical oscillations of the cavity. In normal gravity as the gas jet momentum is increased still further, the oscillations become quite vigorous, and bubbles are formed which become entrained in the bulk liquid. However, these bubbles are driven back up to the liquid surface by buoyancy forces, although new bubbles are continually being formed. The following discussion deals with a situation where gravitational forces are absent and buoyancy forces are nonexistent. Therefore, the impingement phenomena, which include both the stable oscillating gas cavity and the resulting instabilities at large gas momentums, are surface tension dominated.

The gas penetrating into the liquid surface at small momentums resulted in the formation of a stable cavity as shown in figure 4. In figure 4(a), the position of the liquid-gas interface during weightlessness is shown and is completely flat, as it would be under normal gravity conditions. The distance H was experimentally controlled to remain less than three nozzle diameters to minimize jet spreading and velocity decay along the centerline. Although no experimental results for these parabolic profiles appear in the literature, some crude measurements made by the use of a hot-wire anemometer over the range of test Reynolds numbers indicated that a distance of three nozzle diameters would allow the experiments to be conducted with a minimum of velocity decay along the centerline. In figure 4(b), with the initiation of gas impingement, the jet is shown penetrating into the liquid surface. Figures 4(c) and (d) show the formation of a stable cavity under the influence of surface tension.

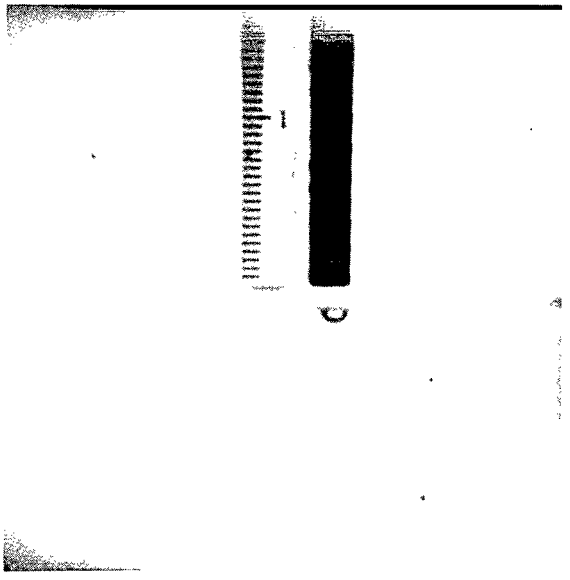

(a) Normal-gravity condition.

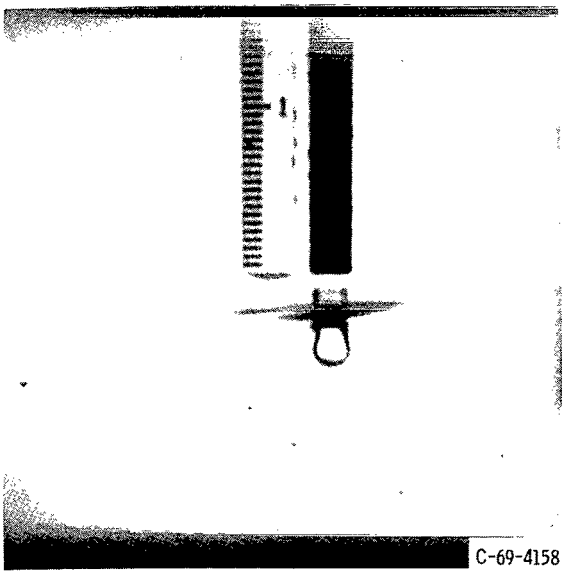

(b) Weightless condition.

Figure 3. - Comparison of gas impingement during weightless and normal-gravity conditions. Average jet velocity, 811 centimeters per second; nozzle diameter, 0.254 centimeter; test liquid, distilled water; distance between nozzle tip and liquid surface, 0.30 centimeter; Reynolds number, 1379.

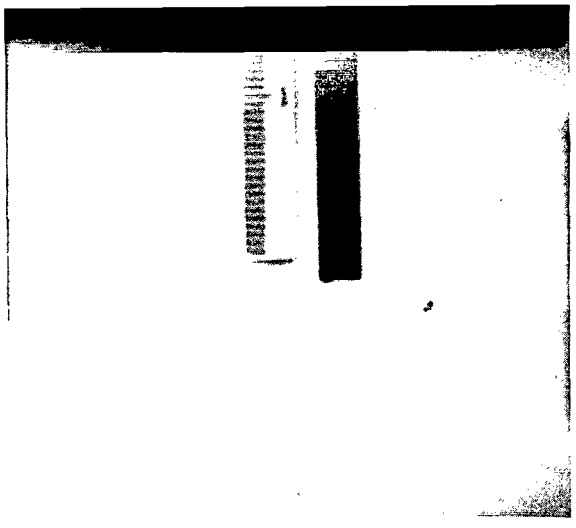

(a) Liquid-gas interface position during weightlessness. Time, 0.53 second.

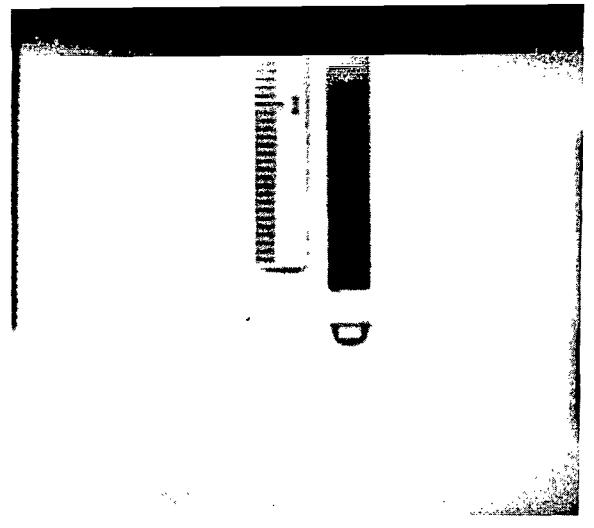

(b) Initiation of gas impingement. Time, 0.57 second.

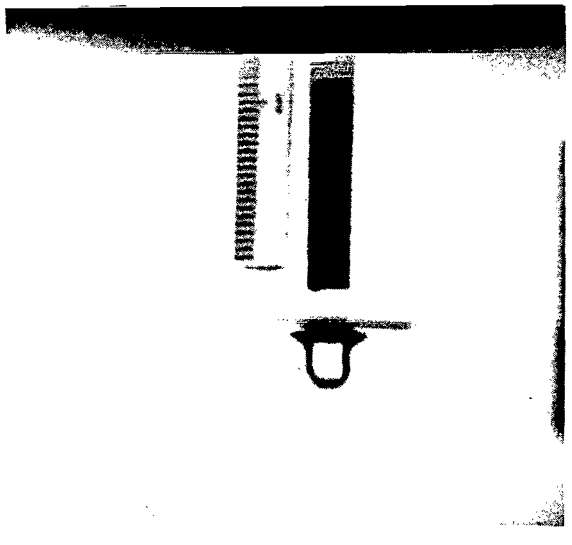

(c) Typical gas cavity shape. Time, 0.80 second.

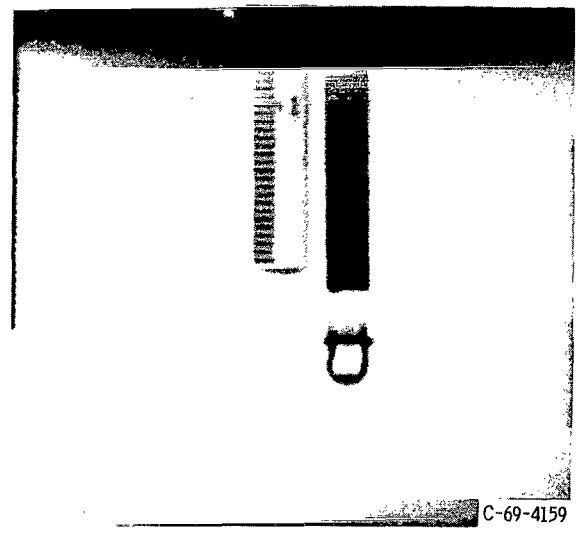

(d) Configuration toward end of test. Time, 1.60 second.

Figure 4. - Gas cavity motion during sample data run. Average jet velocity, 997 centimeters per second; nozzle diameter, 0.254 centimeter; test liquid, distilled water; distance between nozzle tip and liquid surface, 0.53 centimeter; Reynolds number, 1695.

As mentioned previously, for average jet velocities greater than some critical value, bubble pinch-off occurs as indicated in figure 5. The bubbles that pinch off become entrained in the bulk liquid, as shown in figure 5(d). These bubbles either remain in the bulk liquid as single bubbles or coalesce with other bubbles, which is in contrast to their behavior in normal gravity where the bubbles are driven back to the liquid surface. Lar-

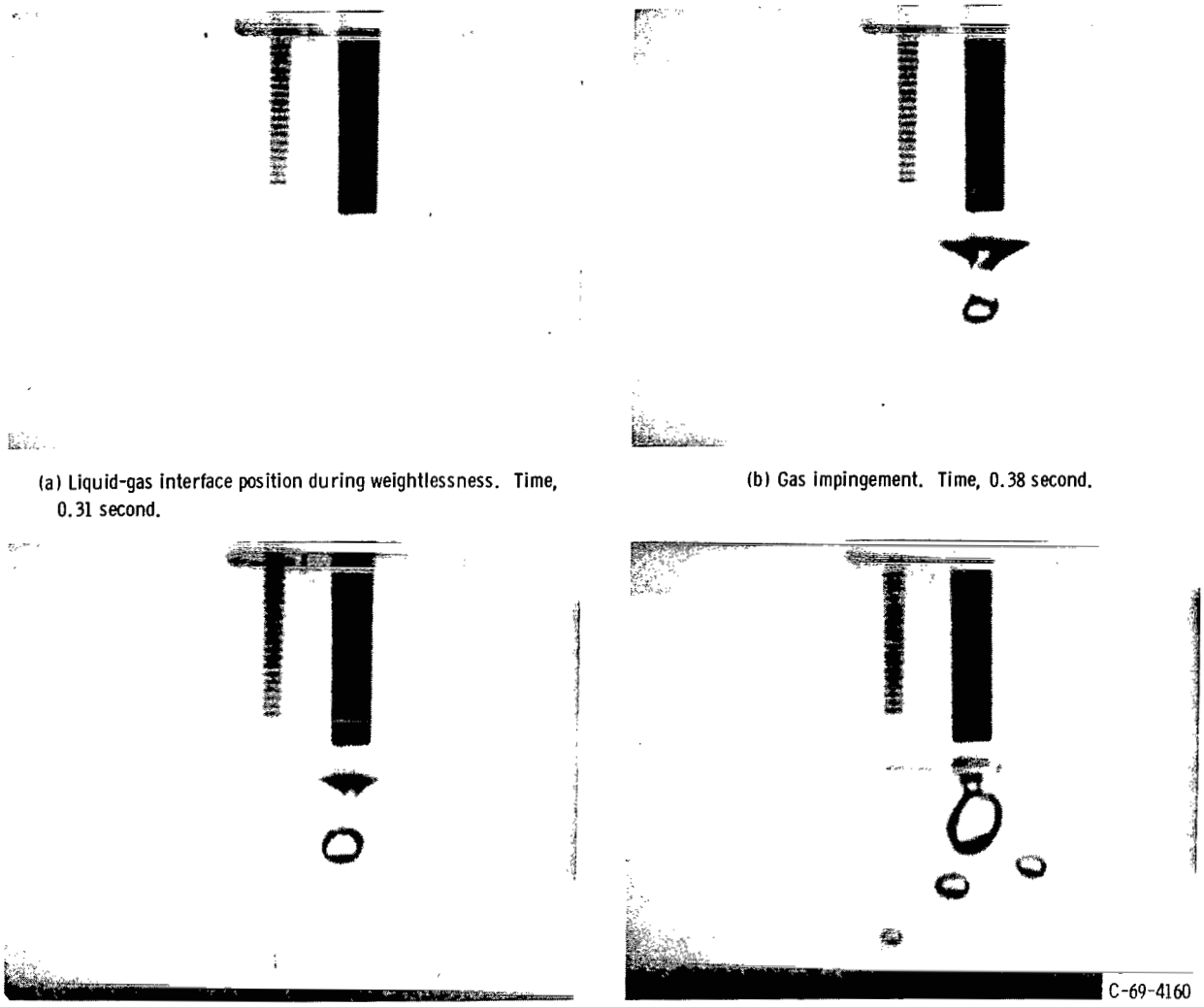

(a) Liquid-gas interface position during weightlessness. Time, 0.31 second.

(b) Gas impingement. Time, 0.38 second.

(c) Bubble pinch-off. Time, 0.57 second.

(d) Configuration near termination of test. Time, 1.79 seconds.

Figure 5. - Occurrence of bubble pinch-off. Average jet velocity, 1260 centimeters per second; nozzle diameter, 0.127 centimeter; test liquid, distilled water; distance between nozzle tip and liquid surface, 0.3 centimeter; Reynolds number, 1071.

ger average jet velocities produce quite different results, as shown in figure 6. In this test, the cavity grew with respect to time, and, in some instances, behavior similar to that indicated in the figure led to liquid engulfing the lower portion of the nozzle. "Spraying" or "sputtering", common instabilities observed in normal gravity gas impingement, were not observed during tests conducted in weightlessness.

Penetration Depth Results

For each test run, the depth of penetration was plotted as a function of the average

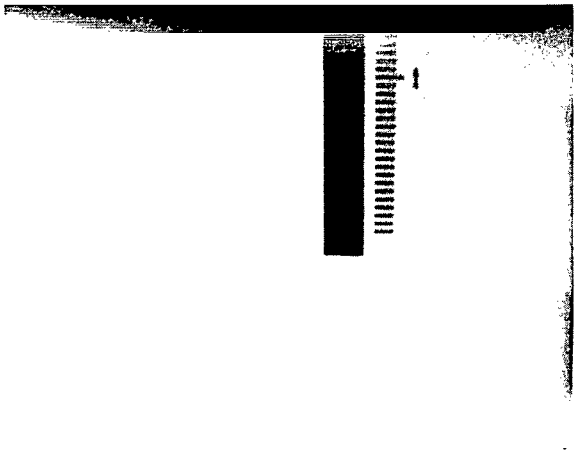

(a) Liquid-gas interface position during weightlessness. Time, 0.45 second.

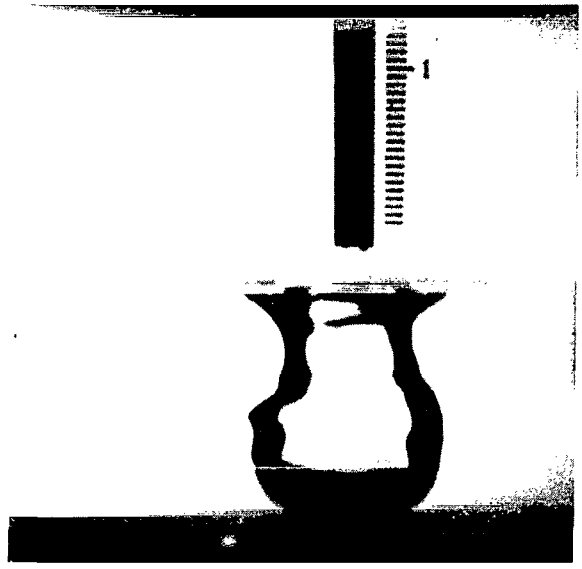

(b) Gas cavity growth. Time, 0.63 second.

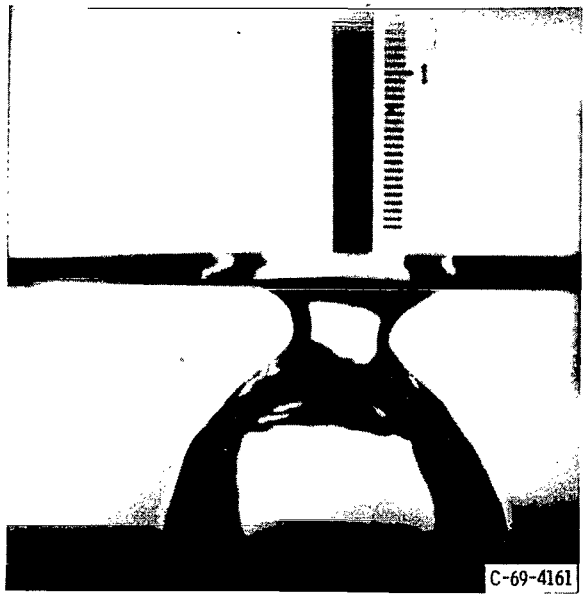

(c) Continuation of cavity growth without bound. Time, 0.89 second.

Figure 6. - Gas cavity growth. Average jet velocity, 2830 centimeters per second; nozzle diameter, 0.254 centimeter; test liquid, distilled water; distance between nozzle tip and liquid surface, 0.68 centimeter; Reynolds number, 4811.

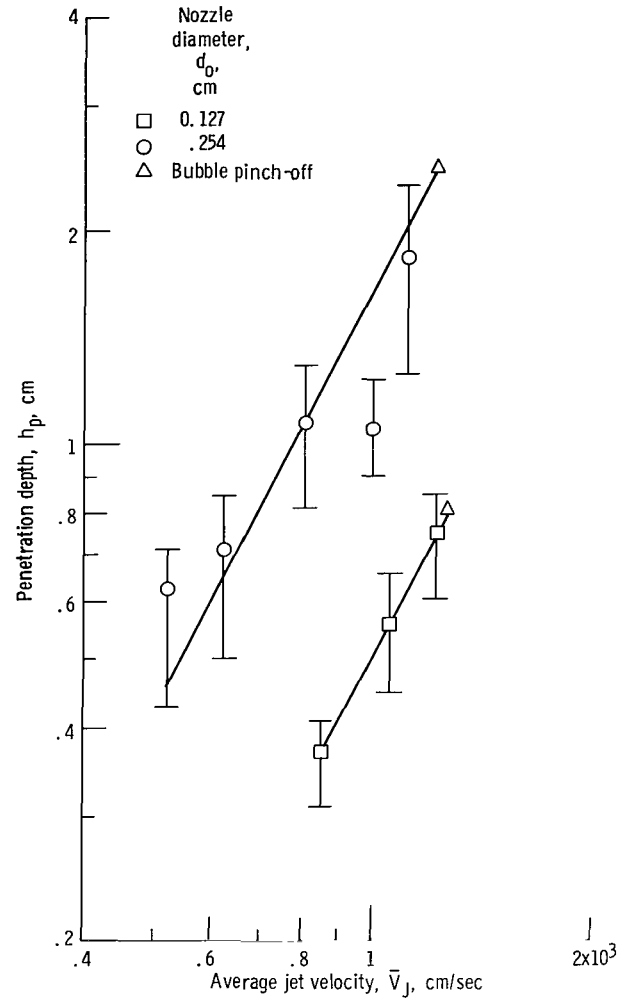

Figure 7. - Gas impingement during weightlessness.

jet velocity, as shown in figure 7. The plots also indicate the extremes in measurements with respect to these depths by means of error bands. Two nozzle diameters were tested, 0.127 and 0.254 centimeter. One immediate result, which can be seen from figure 7, is that, for a constant average jet velocity, the average penetration depth increases with increasing diameter. This result was predicted by the analysis (see eq. (11)). The gas penetration depth increases with the square of the average jet velocity for these initially parabolic profiles until a termination point is reached, as indicated by the triangular symbols. At velocities above this point, instability of the gas cavity occurs with subsequent bubble pinch-off, as described earlier and shown in figures 5 and 6. Any further increase in the average jet velocity results in the formation of more bubbles and, hence, the penetration depth could not be measured for these tests. A correlation for the penetration depth during weightlessness can only be valid for average jet velocities less than

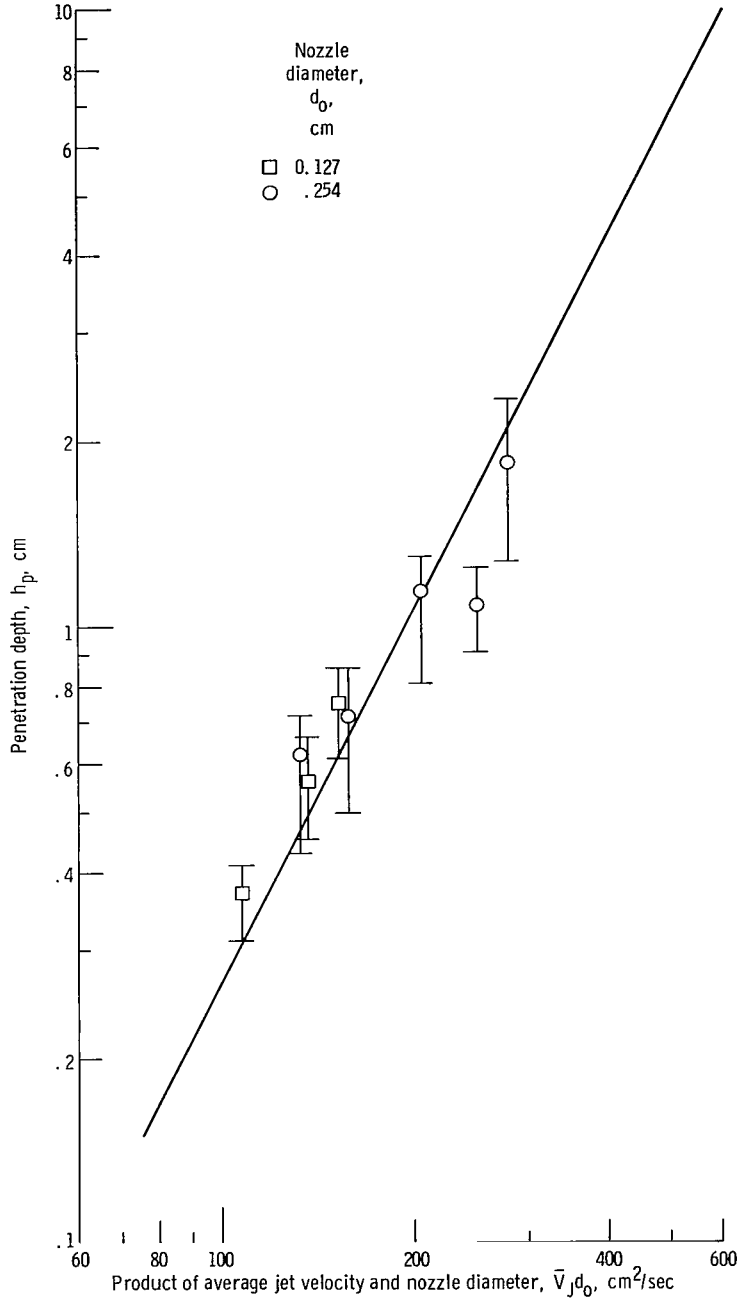

Figure 8. - Effect of jet momentum on penetration depth during weightlessness.

that at which instability (or bubble formation) is initially observed to occur.

A correlation with equation (11) was attempted, and, since surface tension and gas density were invariant in the testing, equation (11) can be rewritten as

$$h_p = \frac{\rho_g}{12\sigma} (\bar{V}_J d_o)^2 = 1.34\times10^{-6} (\bar{V}_J d_o)^2 \tag{13}$$

A plot of penetration depth as a function of the product of the average jet velocity and nozzle diameter is presented in figure 8. A line having a fixed slope of 2 was faired through the data and indicates that they agree well with the analytical form of the parameters and the power to which they are raised. However, the constant calculated empirically from figure 8 is 26.7×10^{-6} as compared with the theoretical value of 1.34×10^{-6}. The main discrepancy between experiment and theory was related to the formulation of the pressure distribution (eq. (5)). First, the pressure distribution was assumed to be similar to that for an initially flat velocity profile with certain modifications. Second, the nonshallow cavities, as realized in the tests conducted, could alter the assumed pressure distribution. Finally, even if the gas cavity is moderately deep, a portion of the exiting gas flow will possess a vertical component of velocity and, hence, of momentum. Thus, it must also be concluded that the net transfer of momentum flux may be somewhat greater than the value given in equation (4). Using the empirical constant of 26.7×10^{-6} allows us to express equation (13) as $h_p = 1.7(\rho_g/\sigma)(\bar{V}_J d_o)^2$.

Possibly, a more meaningful expression for the depth of penetration is one stated in terms of the momentum flux (eq. (12)). This relation can be rewritten employing the experimental data from figure 8, and the equation $M_{par} = 0.6(\sigma h_p)$ is obtained. The reasons for the discrepancy between the theoretical constant of 4π and the empirical constant of 0.6 are similar to those which were involved in the discussion of equation (13).

SUMMARY OF RESULTS

An experimental investigation was conducted to determine the characteristics of a gas jet impinging normally on a liquid surface during weightlessness. The initial velocity profile of the jet exiting from a circular nozzle was completely parabolic, and the liquid surface was located less than three nozzle diameters away to minimize the effects of jet spreading. Distilled water was used as the test liquid, and nozzle diameters of 0.127 and 0.254 centimeter were studied. The contact angle between the distilled water and the test container surface was maintained at 90^o so that the liquid-gas interface remained essentially flat during impingement. The investigation yielded the following results:

1. In weightlessness, the jet penetration depth was correlated with the following an-

alytically developed relation: h_p = constant $\times (\rho_g/\sigma)(\overline{V}_J d_o)^2$, where h_p is the penetration depth, ρ_g is the gas density, σ is the surface tension of the liquid, $\overline{V}_J$ is the average jet velocity, and d_o is the nozzle diameter. The constant in this relation was empirically determined to be 1.7.

2. For large jet momentums, the cavity became unstable. Initially, gas bubbles pinched off from the cavity, and, as the jet momentum was increased further, the cavity grew with respect to time.

3. Spraying or sputtering, which occurs during normal gravity gas impingement, was not observed during weightlessness.

Lewis Research Center,
National Aeronautics and Space Administration,
Cleveland, Ohio, December 10, 1969,
124-09.

APPENDIX - APPARATUS AND PROCEDURE

Test Facility

The experimental data for this study were obtained in the Lewis Research Center's 2.2-Second Zero-Gravity Facility. A schematic diagram of this facility is shown in figure 9. The facility consists of a building 6.4 meters (21 ft) square by 30.5 meters (100 ft) tall. Contained within the building is a drop area 27 meters (89 ft) long with a cross section 1.5 by 2.75 meters (5 by 9 ft).

The service building has a shop and service area, a calibration room, and a controlled environment room. Those components of the experiment that required special handling were prepared in the controlled environment room of the facility. This air-conditioned and filtered room (shown in fig. 10) contains an ultrasonic cleaning system and the laboratory equipment necessary for handling test liquids.

Mode of operation. - A 2.2-second period of weightlessness is obtained by allowing the experiment package to free fall from the top of the drop area. In order to minimize drag on the experiment package, it is enclosed in a drag shield designed with a high ratio of weight to frontal area and a low drag coefficient. The relative motion of the experiment package with respect to the drag shield during a test is shown in figure 11. Throughout the test, the experiment package and drag shield fall freely and independently of each other; that is, no guide wires, electrical lines, etc. are connected to either. Therefore, the only force acting on the freely falling experiment package is the air drag associated with the relative motion of the package within the enclosure of the drag shield. This air drag results in an equivalent gravitational acceleration acting on the experiment, which is estimated to be below 10^{-5} g's.

Release system. - The experiment package, installed within the drag shield, is suspended at the top of the drop area by means of a highly stressed music wire attached to the release system. This release system consists of a double-acting air cylinder with a hard-steel knife edge attached to the piston. Pressurization of the air cylinder drives the knife edge against the wire, which is backed by an anvil. The resulting notch causes the wire to fail, smoothly releasing the experiment. No measurable disturbances are imparted to the package by this release procedure.

Recovery system. - After the experiment package and drag shield have traversed the total length of the drop area, they are recovered by deceleration in a 2.2-meter- (7-ft-) deep container filled with sand. The deceleration rate (averaging 15 g's) is controlled by selectively varying the tips of the deceleration spikes mounted on the bottom of the drag shield (fig. 9). At the time of impact of the drag shield in the decelerator container, the experiment package has traversed the vertical distance within the drag shield (compare figs. 11(a) and (c)).

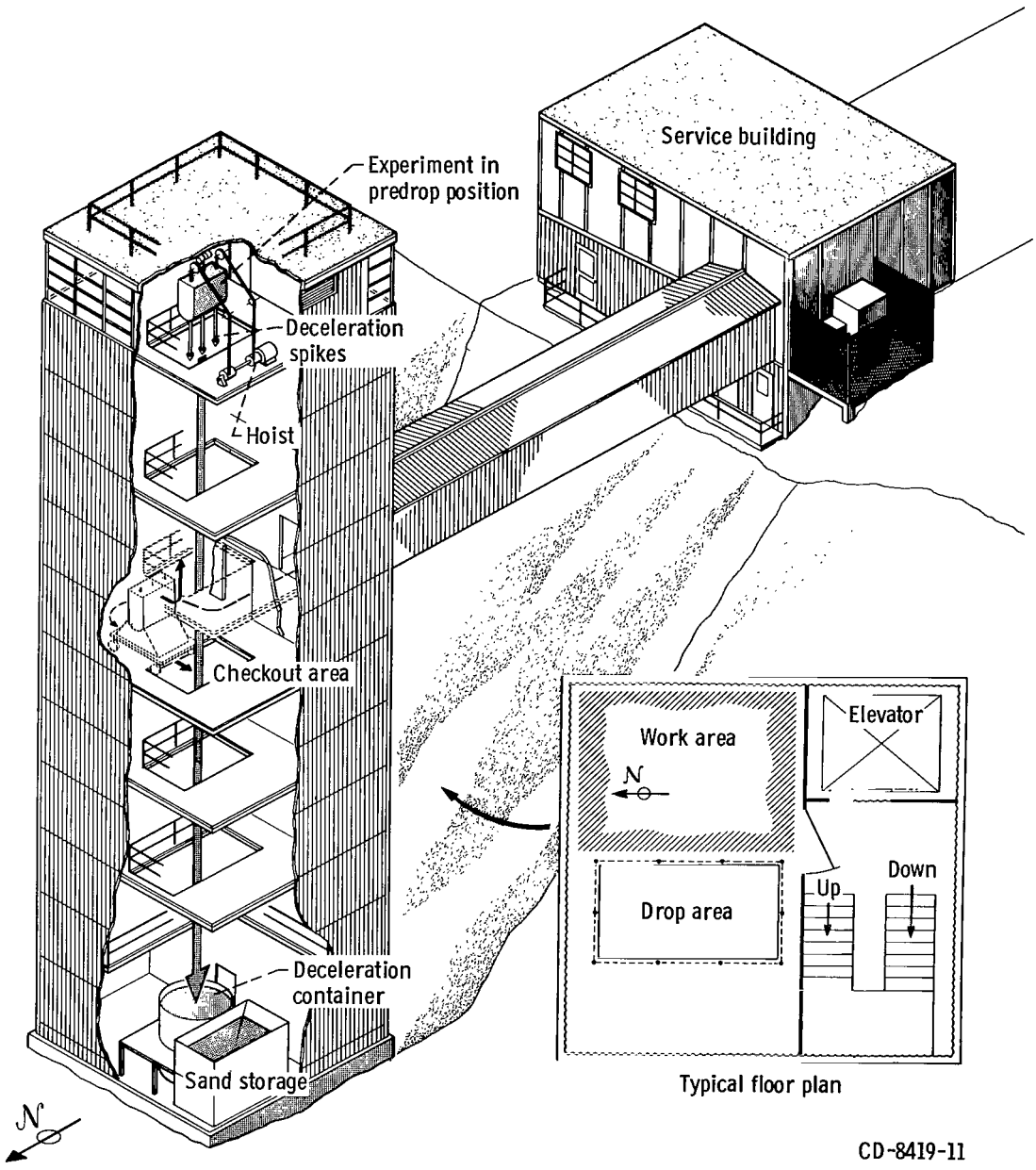

Figure 9. - 2.2-Second Zero-Gravity Facility.

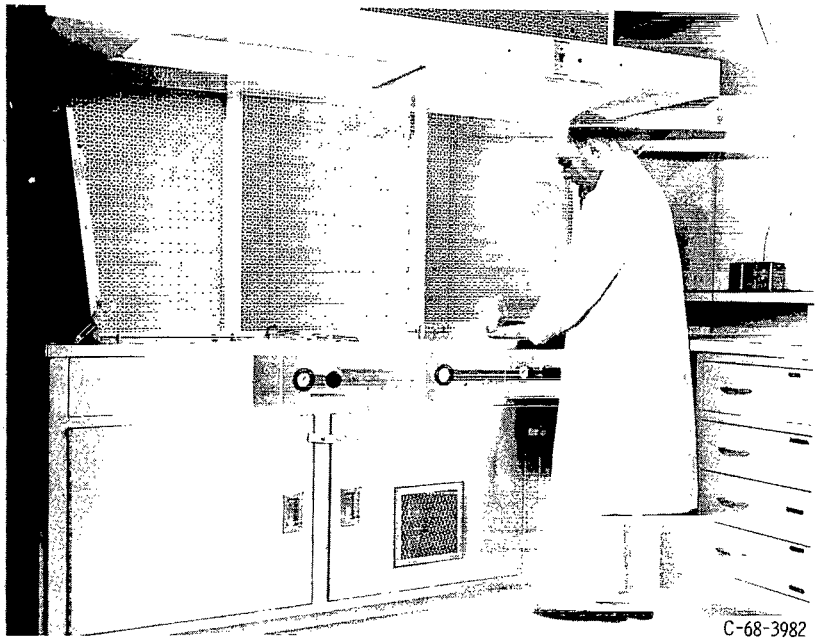

C-68-3982

(a) Ultrasonic cleaning system.

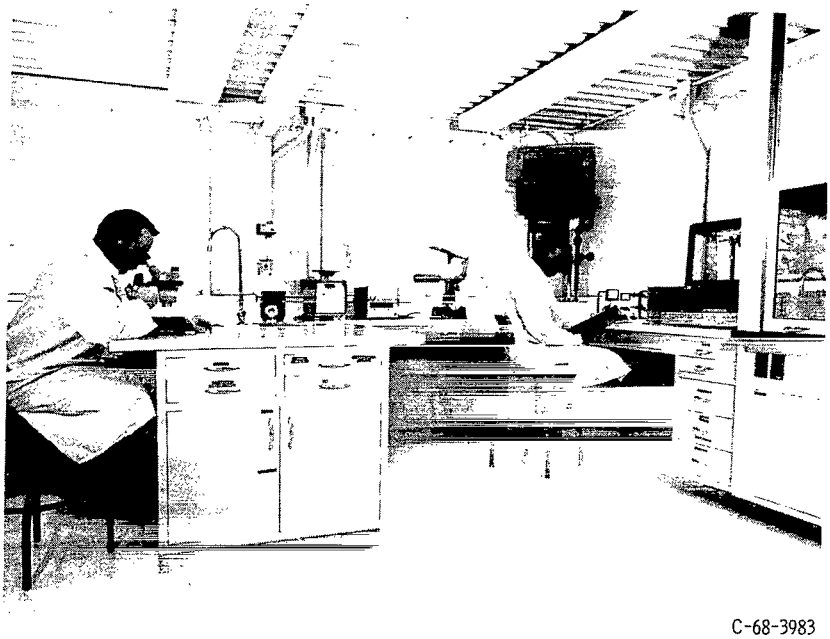

C-68-3983

(b) Laboratory equipment.

Figure 10. - Controlled environment room.

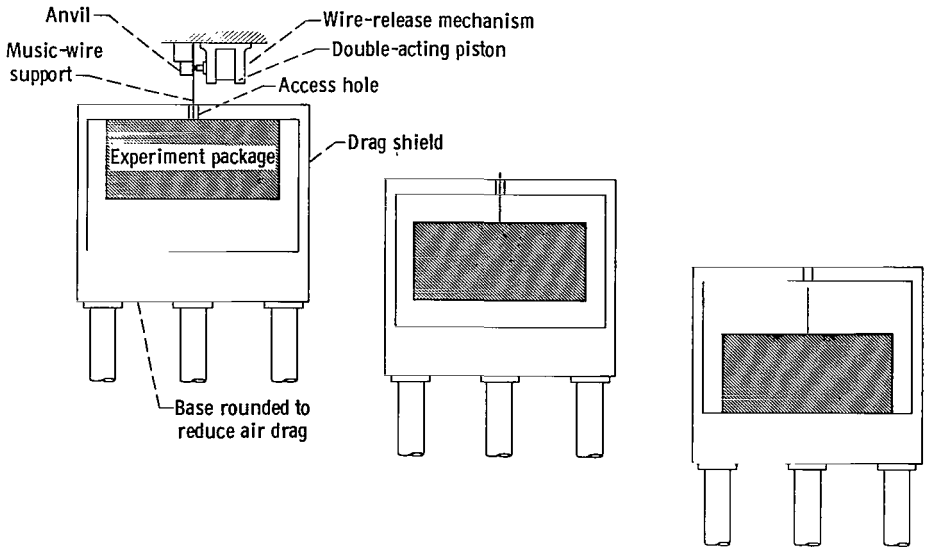

Figure 11. - Position of experiment package and drag shield before, during, and after test drop.

Experiment Package and Test Containers

Experiment package. - The experiment package used to obtain the data for this experimental study is shown in figure 12. It consisted of an aluminum frame in which were mounted the experiment, a circular nozzle, accumulator bottles, a 16-millimeter high-speed motion picture camera, a background lighting scheme, and auxiliary equipment. The auxiliary equipment included batteries, a sequence timer, and a digital clock with divisions of 0.01 second.

Test containers. - A cylindrical tank, 19 centimeters (7.48 in.) in diameter, was fabricated from acrylic plastic and located directly below a circular nozzle. The cylinder was polished until clear and was provided with a plastic top that had a circular hole 4 centimeters (1.6 in.) in diameter for both nozzle placement and gas escape. Marks were etched on the outside of the cylindrical tank for purposes of filling with the test liquid.

Nozzles. - The nozzles were fabricated from brass and had inside diameters of 0.127 and 0.254 centimeter (0.05 and 0.10 in.) The length of the nozzles was 7.62 centimeters (3.0 in.), such that the length-to-diameter ratios were 60 for the smaller nozzle and 30

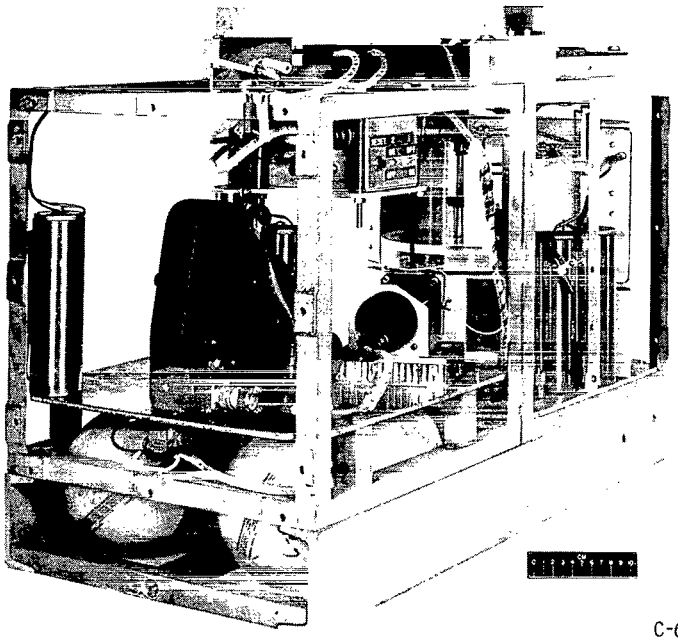

C-69-1850

Figure 12. - Experiment package.

for the larger. The inside diameters of these nozzles were machined so that they were concentric to within 0.00127 centimeter (0.0005 in.). The tips of the nozzles were machined to have a square edge. They were designed with a 1.27-centimeter (0.5-in.) conically shaped entrance length so that, in conjunction with the length-to-diameter ratios, the flow exiting from the nozzle had an initially parabolic profile. These nozzles were located directly above the plastic tank (fig. 12) and were alined with premachined lines on the test rig so that the centerline of each nozzle was perpendicular to the liquid surface.

Test Procedure

Experiment preparation. - Prior to a test run, the experiment tank was cleaned ultrasonically with a mild detergent. After the tank was rinsed with methanol, it was dried in a warm air dryer. After drying, the interior surface of the tank wall was coated with an organosilicon product to absorb traces of water and then sprayed with polytetrafluoroethylene. It was found that a rapid wiping of this spray from the container surface with paper towels and immediate polishing was a good procedure for obtaining a 90° contact angle with the surface in contact with distilled water. The surface was subsequently resprayed and repolished as deemed necessary. The tank was then rinsed and filled with distilled water to a predetermined mark located on the outside of the test tank. This mark was determined by the required nozzle-tip to liquid-surface distance. Distilled

water was the only test liquid that could be found that would permit a 90^{o} contact angle to be maintained. This angle was the most desirable since the resulting formation time from a normal gravity to a weightless environment is zero. Other contact angles require finite formation times for the liquid to reach a static equilibrium configuration. Especially in cylinders with a diameter of 19 centimeters (7.48 in.), the choice of other angles would not be feasible for obtaining a quiescent liquid-gas interface prior to gas impingement.

The required mass flow rate through the circular nozzle was calibrated on the ground. Dry nitrogen was employed as the test gas at 50 psi (3.45×10^{5} N/m^{2}). The flow through the nozzle was controlled by means of a micrometer located on the rig. The flow passed through calibrated rotometers in the specific flow rate range desired. It was assumed that the density of the exiting gas was the same value at atmospheric pressure and temperature. Two accumulator bottles located on the test rig were filled with nitrogen to a pressure of 50 psi (3.45×10^{5} N/m^{2}) just prior to the drop. The accumulator bottles were of sufficient volume so that no decrease in pressure was observed, as determined by a gage located aboard the test rig and checked at the termination of the drop. A small time increment (of the order of 0.4 sec) was allowed prior to gas impingement so that any deviation from a 90^{o} contact angle (which would invalidate the test run) would be detected on the film.

Procedure for test drop. - Electrical timers on the experiment package were set to control the initiation and duration of all functions programmed during the drop. The experiment package was then balanced and positioned within the prebalanced drag shield. The wire support was attached to the experiment package through an access hole in the shield (see fig. 11(a)). Properly sized spike tips were installed on the drag shield. Then the drag shield, with the experiment package inside, was hoisted to the predrop position at the top of the facility (fig. 9) and connected to an external electrical power source. The wire support was attached to the release system, and the entire assembly was suspended from the wire. After final electrical checks were made and the experiment package was switched to internal power, the system was released. After completion of the test, the experiment package and drag shield were returned to the preparation area.

REFERENCES

1. Banks, Robert B.; and Chandrasekhara, D. V.: Experimental Investigation of the Penetration of a High-Velocity Gas Jet Through a Liquid Surface. J. Fluid Mech., vol. 15, pt. 1, Jan. 1963, pp. 13-34.
2. Blackmon, J. B.: Pressurization Gas Flow Effects on Liquid Interface Stability. DAC-60711, Douglas Aircraft Co., July 1967.
3. Struck, H. G.: Jet Penetration into a Liquid. NASA TM X-53214, 1965.
4. Hopkins, D. F.; and Robertson, J. M.: Two-Dimensional Incompressible Fluid Jet Penetration. J. Fluid Mech., vol. 29, pt. 2, Aug. 11, 1967, pp. 272-287.
5. Andrade, E. N. da C.; and Tsien, L. C.: The Velocity-Distribution in a Liquid-into-Liquid Jet. Proc. Phys. Soc., vol. 49, pt. 4, July 1937, pp. 381-391.
6. Shames, Irving H.: Mechanics of Fluids. McGraw-Hill Book Co., Inc., 1962.
7. Gibson, Arnold H.: Hydraulics and Its Applications. Dover Publ., Inc., 1952.
8. Schlichting, Hermann (J. Kestin, trans.): Boundary Layer Theory. Fourth ed., McGraw-Hill Book Co., Inc., 1960.

NASA-Langley, 1970 —— 12 E-5438

"The aeronautical and space activities of the United States shall be conducted so as to contribute . . . to the expansion of human knowledge of phenomena in the atmosphere and space. The Administration shall provide for the widest practicable and appropriate dissemination of information concerning its activities and the results thereof."

—NATIONAL AERONAUTICS AND SPACE ACT OF 1958

NASA SCIENTIFIC AND TECHNICAL PUBLICATIONS

TECHNICAL REPORTS: Scientific and technical information considered important, complete, and a lasting contribution to existing knowledge.

TECHNICAL NOTES: Information less broad in scope but nevertheless of importance as a contribution to existing knowledge.

TECHNICAL MEMORANDUMS: Information receiving limited distribution because of preliminary data, security classification, or other reasons.

CONTRACTOR REPORTS: Scientific and technical information generated under a NASA contract or grant and considered an important contribution to existing knowledge.

TECHNICAL TRANSLATIONS: Information published in a foreign language considered to merit NASA distribution in English.

SPECIAL PUBLICATIONS: Information derived from or of value to NASA activities. Publications include conference proceedings, monographs, data compilations, handbooks, sourcebooks, and special bibliographies.

TECHNOLOGY UTILIZATION PUBLICATIONS: Information on technology used by NASA that may be of particular interest in commercial and other non-aerospace applications. Publications include Tech Briefs, Technology Utilization Reports and Notes, and Technology Surveys.

Details on the availability of these publications may be obtained from:

SCIENTIFIC AND TECHNICAL INFORMATION DIVISION

NATIONAL AERONAUTICS AND SPACE ADMINISTRATION

Washington, D.C. 20546